Available online at www.sciencedirect.com

ScienceDirect

Ceramics International 40 (2014) 1865–1872

CERAMICS INTERNATIONAL

www.elsevier.com/locate/ceramint

Proton-conducting $Ba_{1-x}K_xCe_{0.6}Zr_{0.2}Y_{0.2}O_{3-\delta}$ oxides synthesized by sol–gel combined with composition-exchange method

Kan-Rong Lee[a,b], Yen-Chun Chiang[c], I-Ming Hung[c], Chung-Jen Tseng[b], Jeng-Kuei Chang[a], Sheng-Wei Lee[a,*]

[a]Institute of Materials Science and Engineering, National Central University, Jhongli City 32001, Taiwan, ROC
[b]Department of Mechanical Engineering, National Central University, Jhongli City 32001, Taiwan, ROC
[c]Department of Chemical Engineering and Materials Science, Yuan Ze University, Jhongli City 32003, Taiwan, ROC

Received 20 June 2013; received in revised form 17 July 2013; accepted 17 July 2013
Available online 24 July 2013

Abstract

This study reports the synthesis of proton-conducting $Ba_{1-x}K_xCe_{0.6}Zr_{0.2}Y_{0.2}O_{3-\delta}$ ($x=0.025$–0.075) ceramics by using a combination of citrate–EDTA complexing sol–gel process and the composition-exchange method. Compared to the sintered oxides of similar composition prepared from conventional sol–gel powders, $Ba_{1-x}K_xCe_{0.6}Zr_{0.2}Y_{0.2}O_{3-\delta}$ oxides synthesized by sol–gel combined with the composition-exchange method are found to exhibit improved sinterability, higher conductivity, more homogeneous phase, and excellent chemical stability against CO_2. Among all sintered oxides in this study, the $Ba_{0.925}K_{0.075}Ce_{0.6}Zr_{0.2}Y_{0.2}O_{3-\delta}$ pellet fabricated by this new method has the highest conductivity, 0.0094 S/cm at 800 °C, which is higher than those pressed from conventional sol–gel powders in the K doping range of 0–15%. Based on the experimental results, we discuss the mechanism for improvement in these properties in terms of calcined particle characteristics. This work demonstrates that $Ba_{1-x}K_xCe_{0.6}Zr_{0.2}Y_{0.2}O_{3-\delta}$ oxides synthesized by sol–gel combined with the composition-exchange method would be a promising electrolyte for H^+-SOFC applications. More importantly, this new fabrication approach may be applied to other similar material systems, such as Sr-doped $Ba(Ce,Zr)O_3$ ceramics.

Keywords: C. Ionic conductivity; Proton-conducting electrolyte; Solid oxide fuel cells; $Ba_{1-x}K_xCe_{0.6}Zr_{0.2}Y_{0.2}O_{3-\delta}$; Chemical stability

1. Introduction

Solid oxide fuel cells (SOFCs) have been recognized as high-efficient and clean power-generation devices due to their high thermodynamic efficiency, low environmental impact, and possibility of internal reforming of the fuel [1–3]. Traditional SOFCs are composed of oxygen-ion-conducting electrolytes (O^{2-}-SOFCs) and usually require operation at approximately 1000 °C. Such a high operation temperature introduces many practical problems, such as high costs, materials degradations, thermal expansion mismatch, reactions between the components, slow start-up and shut-off, [4,5] etc. Therefore, there is increasing interest in developing SOFCs based on proton-conducting electrolytes (H^+-SOFCs) operating at an intermediate temperature range of 400–800 °C that facilitates the selection of sealing and interconnection materials, control of the interactions between the electrode/electrolyte, and thereby prolongs the operational lifetime of devices [6–8]. Moreover, H^+-SOFCs have higher theoretical electromotive force (EMF) and electrical efficiency than O^{2-}-SOFCs [9]. The key issue in the development of H^+-SOFC is the use of a highly proton-conductive electrolyte with sufficient thermal stability at intermediate temperatures in various environments.

Perovskite-type oxides including $BaCeO_3$, $BaZrO_3$, $SrCeO_3$, and $SrZrO_3$ have been reported to exhibit predominant proton conduction at elevated temperature in hydrogen containing or humidified atmosphere [10]. Among these proton-conductive electrolytes, $BaCeO_3$-based oxides are generally believed to have the highest conductivity [11]. However, their chemical instability has been confirmed under CO_2, H_2O, or H_2S containing atmosphere at high temperature [12–14]. Unfavorable reactions with

*Correspondence to: Institute of Materials Science and Engineering, National Central University, No. 300, Jhongda Rd., Jhong-Li City, Taoyuan County 32001, Taiwan, ROC. Tel.: +886 3 4227151x34905; fax: +886 3 2805034.
E-mail address: schon0911@gmail.com (S.-W. Lee).

0272-8842/$ - see front matter © 2013 Elsevier Ltd and Techna Group S.r.l. All rights reserved.
http://dx.doi.org/10.1016/j.ceramint.2013.07.089

carbon species and H_2S could lead to the decomposition of $BaCeO_3$-based electrolyte and performance degradation of H^+-SOFCs. Many efforts have been devoted to partially substitute Ce with Zr in the hope to improve the chemical stability [15–17]. In addition, to enhance the protonic conduction in $BaCe_{1-x}Zr_xO_3$, doping with lower-valence cations is also essential. A trivalent dopant such as Y^{3+} can lead to the creation of oxygen vacancies, thus resulting in enhanced protonic conduction. Many studies have reported the promising performance of proton-conducting $BaCe_{1-x-y}Zr_xY_yO_{3-\delta}$ since it maintains the good chemical stability of $BaZrO_3$ but with improved electrical conductivity compared to $BaCe_{1-x}Zr_xO_3$ [18–20].

Several synthesis techniques have been utilized to prepare $BaCe_{1-x-y}Zr_xY_yO_{3-\delta}$ powders, including solid-state reaction [21], combustion [22], sol–gel [23], etc. The sol–gel process has gained considerable attention because it can produce powders with great compositional uniformity, low residual carbon level, and nano-scale particle size [16,24], which is important to make dense products at lower sintering temperatures. In addition, the nano-crystalline conductors have been reported to have higher conductivity compared to micro-scale oxides prepared using other processes due to favorable ionic mobility along the grain boundaries [25]. On the other hand, protonic conductivity of perovskites is found to be strongly affected by the basicity of the constituent oxides due to its dominant influence on water uptake capacity [10]. Therefore, introducing highly basic alkaline cations into perovskite oxides should further improve the protonic conductivity. A significantly higher conductivity has been shown in K-doped $BaZrO_3$ than that in undoped $BaZrO_3$ [26]. Xu et al. also demonstrated that the water uptake of Y-doped $BaZrO_3$ synthesized by solid state reaction was increased with 5% K doped at the A-site of perovskites [27]. However, both works found that introducing K into perovskites may lead to poor sinterability, high porosity, and second phase formation, possibly due to the limit of K doping at A-site and high volatility of K-doped oxide at high process temperatures. In this study, we first report the synthesis of proton-conducting $Ba_{1-x}K_xCe_{0.6}Zr_{0.2}Y_{0.2}O_{3-\delta}$ ($x=0.025$–0.075) ceramics by using a combination of citrate–ethylenediaminetetraacetic acid (EDTA) complexing sol–gel process and the composition-exchange method. Compared to those sintered oxides of similar composition prepared from conventional sol–gel powders, $Ba_{1-x}K_xCe_{0.6}Zr_{0.2}Y_{0.2}O_{3-\delta}$ oxides synthesized by sol–gel combined with the composition-exchange method are found to exhibit improved sinterability, higher conductivity, more homogeneous phase, and excellent chemical stability against CO_2. Based on the experimental results, the mechanism for improvement in these properties is discussed in terms of calcined particle characteristics.

2. Experimental procedure

In this study, $Ba_{1-x}K_xCe_{0.6}Zr_{0.2}Y_{0.2}O_{3-\delta}$ ($x=0.025$–0.075) oxides were prepared by using a citrate–EDTA complexing sol–gel method combined the composition-exchange process. The starting materials were commercial $Ba(NO_3)_2$ (J.T. Baker, 99.3%), KNO_3 (J.T. Baker, 99.9%), $ZrO(NO_3)_2\cdot 2H_2O$ (Showa, 99.0%), $Ce(NO_3)_3\cdot 6H_2O$ (Alfa Aesar, 99.5%), and $Y(NO_3)_3\cdot 6H_2O$ (Alfa Aesar, 99.9%). Both citric acid and EDTA were used as chelating agents to complex metal cations. The molar ratio of citric acid and EDTA to the total metal cations content was set at 2:2:3. The pH value of the solution was adjusted to be around 6 using NH_4OH. The mixed solutions were heated to 100 °C under stirring until viscous gels were obtained. After further heating at 250 °C to evaporate residual water and organics, these gels were converted into black powders. The synthesized powders were then calcined at 1000 °C for 12 h with a heating rate of 5 °C/min. Subsequently, the calcined powders with the nominal K doping of 5%, 10%, and 15% were separately mixed with the non-doped powders (by the molar ratio of 1:1) and uniformly stirred in 95% ethanol for 3 h to attain the so-called composition-exchange powders with an equivalent nominal K content of 2.5%, 5%, and 7.5%. To obtain dense ceramics, all as-calcined and mixed powders were uniaxially pressed into cylindrical pellets (1 cm in diameter and 1 mm in thickness) at 250 MPa for 20 s and then sintered in air atmosphere. Sintering was carried out at 1600 °C for 4 h. In the following discussion, we refer to the sintered pellets pressed from sol–gel combined with composition-exchange powders as CE-1 (2.5% K), CE-2 (5% K), and CE-3 (7.5% K) samples.

The phase identification of the sintered ceramics was performed with a powder diffractometer (Bruker D8A) with Ni-filtered Cu Kα radiation and the diffraction angle from 20° to 80° with a step of 0.01°. Surface morphologies of the calcined and sintered oxides were examined using a field-emission scanning electron microscope (FESEM, FEI Quanta 200F) in conjunction with an energy dispersion spectrometer (EDS). Relative densities of the sintered pellets were determined by the Archimedes method using water as the liquid medium and the direct measurements of the regular geometric volume and the corresponding mass. In addition, in-situ temperature-dependent dilatometry was used to analyze the densification temperature of calcined $Ba_{1-x}K_xCe_{0.6}Zr_{0.2}Y_{0.2}O_{3-\delta}$ oxides. To further study the local configuration of chemical bonding in $Ba_{1-x}K_xCe_{0.6}Zr_{0.2}Y_{0.2}O_{3-\delta}$ ceramics, Raman spectra were acquired using an Andor SR-500i spectrometer with a spectral resolution of 0.5 cm^{-1}. The Raman spectra were excited by a diode-pumped solid-state (DPSS) laser line with wavelength of 532 nm in a near-backscattering geometry. Raman signal mapping was also performed within a 200 μm × 200 μm area on the sintered pellets with a spatial resolution of 1 μm. The conductivities of the sintered pellets were measured by a dc two-probe method; the measurements were performed in air with 3% relative humidity in the temperature range of 400–800 °C. Silver ink was painted on both faces of the pellets to create current collectors and the measurement data were acquired using an Agilent 34970A meter. Finally, the chemical stability of sintered pellets was evaluated by exposing the sintered pellets to the CO_2 ambient (99.99%) at 600 °C for 16 h.

3. Results and discussion

As shown in Fig. 1a, all sintered $Ba_{1-x}K_xCe_{0.6}Zr_{0.2}Y_{0.2}O_{3-\delta}$ pellets are predominantly the perovskite-type cubic structure, showing five major diffraction signals, namely those from the

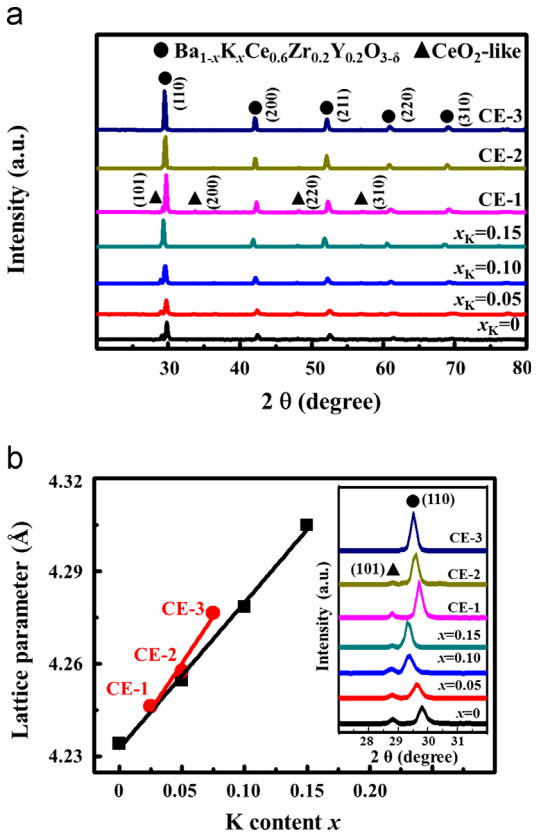

Fig. 1. (a) XRD patterns of the sintered $Ba_{1-x}K_xCe_{0.6}Zr_{0.2}Y_{0.2}O_{3-\delta}$ oxides with varied K doping content fabricated by various methods. (b) Lattice constants of the sintered $Ba_{1-x}K_xCe_{0.6}Zr_{0.2}Y_{0.2}O_{3-\delta}$ oxides as a function of K doping contents based on cubic lattice symmetry. The inset shows enlarged XRD spectra of (a) around 30°.

(110), (200), (211), (220), and (310) planes (JCPDS Card no. 89-2485). Four very weak peaks associated with the cubic (Zr,Ce,Y)O_2-like structure indicated by "▲" are also observed in Fig. 1a. These peaks most possibly correspond to a CeO_2-like phase since their XRD peaks are close to main peaks of CeO_2 [28]. To further verify the formation of the solid solution over the range of K doping ($0.0 \le x \le 0.015$), the lattice constants were determined from XRD analysis based on cubic lattice symmetry and the results are shown in Fig. 1b. For the sintered pellets prepared either from conventional sol–gel powders or from sol–gel combined with composition-exchange powders, a nearly linear relation between lattice parameter and K doping content is observed. Since K^+ (1.38 Å) has only slightly larger ionic radius than Ba^{2+} (1.35 Å) at the A-site of perovskite [29], there exists another mechanism responsible for the variation of lattice parameter with K doping. It has been reported that an addition of K atoms into perovskite-type materials can stabilize the perovskite structure in terms of increased tolerance factor and enhanced electronegativity difference [30,31]. Therefore, we speculate that with an increase in the K doping, the perovskite structure of $Ba_{1-x}K_xCe_{0.6}Zr_{0.2}Y_{0.2}O_{3-\delta}$ oxides can be more stabilized in sintering and in the meanwhile, the formation of CeO_2-like second phase is more suppressed. Under the circumstances, Ce^{4+} cations (0.87 Å) tend to remain at the B-site of perovskite and their larger ionic radius than Zr^{4+} (0.72 Å) results in an increase in lattice parameter [28]. This inference is also consistent with the XRD results shown in the inset of Fig. 1b, in which the CeO_2-like peak appears to diminish with the increasing K doping. We also observe that the sintered pellets pressed from sol–gel combined with composition-exchange powders have a shaper slope in the relation between lattice parameter and K doping. It implies that the formation of CeO_2-like phase in sintered oxides can be further suppressed through the composition-exchange process for the calcined powders.

Fig. 2a–d shows surface morphologies of the sintered $Ba_{1-x}K_xCe_{0.6}Zr_{0.2}Y_{0.2}O_{3-\delta}$ pellets prepared from conventional sol–gel powders. We find that the grain size significantly increases with increasing K doping. Meanwhile, an increasing number and size of pores are observed on the pellet surface. These pores can be ascribed to the oxide volume shrinkage, which results from the release of structural water and residual organics, and volatilization of K-doped oxide at high sintering temperature [26]. Here, we note that the sintered pellet with 20% K doping content was not successfully fabricated due to its high porosity. These results indicate that adding K into $Ba_{1-x}K_xCe_{0.6}Zr_{0.2}Y_{0.2}O_{3-\delta}$ oxides would lead to poor sinterability and high porosity in sintering. On the other hand, the CE-3 sample (prepared from sol–gel combined with composition-exchange powders) seems considerably densified and very few pores can be seen on the pellet surface (see Fig. 2e). Fig. 2f shows the representative SEM micrograph taken from the fractured cross-section of the CE-3 sample. The image shows that the interior structure is also well densified, indicating an obvious improvement in sinterability of the powders synthesized by sol–gel combined with the composition-exchange method. In addition, the relative densities of these sintered pellets are also summarized in Fig. 3. The relative densities for the pellets sintered from conventional sol–gel powders significantly decrease with increasing K doping. Nevertheless, relative densities higher than 97% can be achieved for all pellets sintered from sol–gel combined with composition- exchange powders. Such compact and dense $Ba_{1-x}K_xCe_{0.6}Zr_{0.2}Y_{0.2}O_{3-\delta}$ oxides (not fuel-permeable) could be a suitable electrolyte for the use in H^+-SOFCs.

We attempt to discuss the mechanism for the above-discussed improvement in terms of calcined particle characteristics. Fig. 4a and c shows the SEM images of conventional sol–gel calcined powders with 0% and 15% K doping, respectively. The K doping content significantly affects the particle size of calcined powders. The calcined powders with 15% K doping have particle size ranging from 350 to 900 nm, which is much larger than that of the non-doped powders, ~85 nm in average. The larger-particle size and correspondingly larger gaps between particles can provide pathways for the release of structural water and volatilization of K-based oxide, leading to higher porosity in the sintered pellets as seen in Fig. 2d. On the other hand, the CE-3 calcined powders prepared through the composition-exchange process (see Fig. 4b) exhibit bimodal particle size distribution since it is a mixture of two respective K-doped powders. We speculate that the smaller calcined particles can fill the gaps between the larger particles

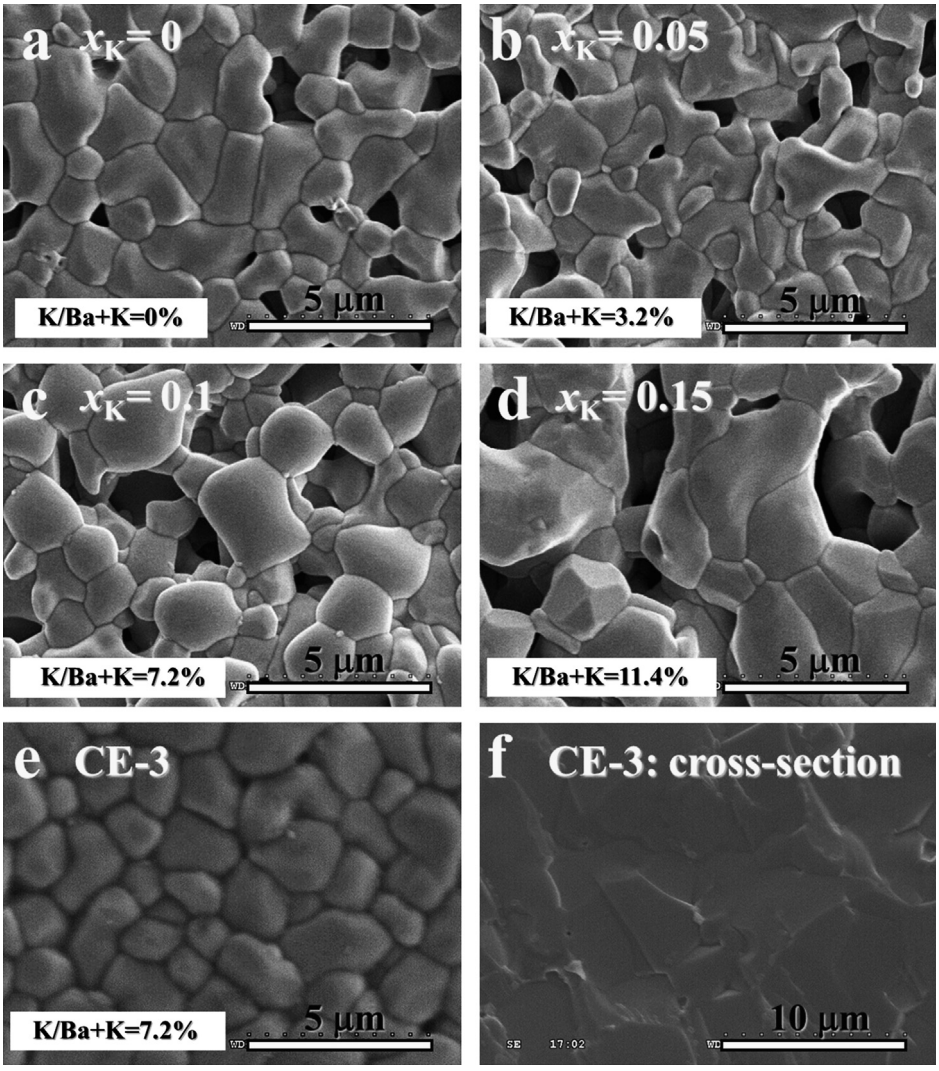

Fig. 2. SEM images of surface morphologies of the $Ba_{1-x}K_xCe_{0.6}Zr_{0.2}Y_{0.2}O_{3-\delta}$ pellets with (a) $x=0$, (b) $x=0.05$, (c) $x=0.1$, (d) $x=0.15$, from conventional sol–gel powders, and (e) $x=0.075$ prepared from sol–gel combined with composition-exchange powders (the CE-3 sample). (f) Fractured cross-section view of the CE-3 pellet.

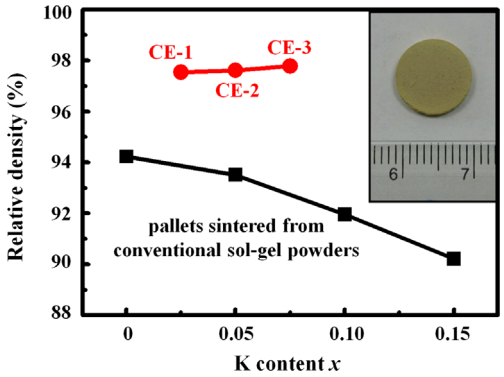

Fig. 3. Relative densities for the sintered $Ba_{1-x}K_xCe_{0.6}Zr_{0.2}Y_{0.2}O_{3-\delta}$ pellets obtained from conventional sol–gel or sol–gel combined with composition-exchange powders. The inset also shows a photograph of a sintered $Ba_{1-x}K_xCe_{0.6}Zr_{0.2}Y_{0.2}O_{3-\delta}$ ($x=0.15$) pellet prepared from sol–gel combined with composition-exchange powders.

through the composition-exchange process. The CE-3 pellet pressed from such mixed powders may give fewer pathways for the release of structural water and volatilization of K-based oxide during sintering, thus resulting in an improvement in sinterability and a considerably dense structure in sintered pellet. This can also well explain why the loss of K doping in the CE-3 pellet (~4%, calculated from the EDS result in Fig. 2e) is smaller than those of samples prepared from conventional sol–gel powders (more than 20%). Fig. 5 also shows the temperature-dependent linear shrinkage measurements upon heating for the pellets pressed from various calcined powders. We find that an increase in the K doping content significantly elevates the densification temperature of the $Ba_{1-x}K_xCe_{0.6}Zr_{0.2}Y_{0.2}O_{3-\delta}$ pellets pressed from conventional sol–gel powders. This is also consistent with the conventional wisdom that finer powders are crucial for fabricating dense ceramics at lower sintering temperature. We further observe that the pellets pressed from sol–gel combined with composition-exchange powders have a lower densification temperature compared to those with the similar nominal K doping prepared from conventional sol–gel powders. This indicates that an appropriate bimodal size distribution of calcined particles through the composition-exchange process is more beneficial for fabricating dense ceramic oxides at lower sintering temperature.

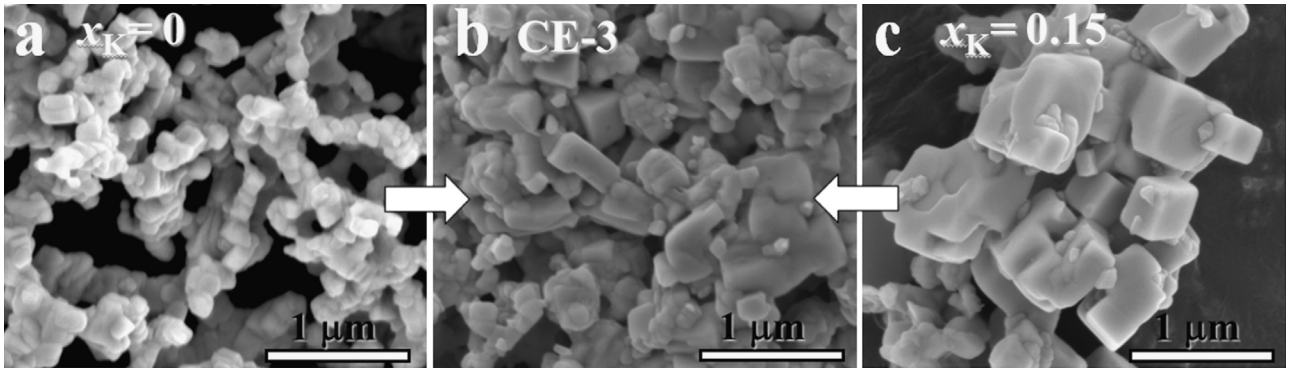

Fig. 4. SEM micrographs of (a) non-doped, (b) CE-3, and (c) 15%-K-doped calcined $Ba_{1-x}K_xCe_{0.6}Zr_{0.2}Y_{0.2}O_{3-\delta}$ powders.

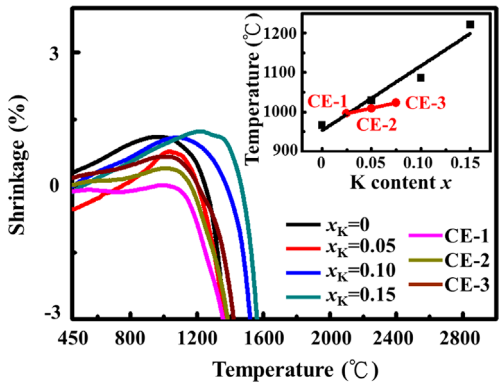

Fig. 5. Linear shrinkage vs. temperature of the calcined $Ba_{1-x}K_xCe_{0.6}Zr_{0.2}Y_{0.2}O_{3-\delta}$ oxides with different K dopings pressed from conventional sol–gel or sol–gel combined with composition-exchange powders. The calcined sample thickness is 1 mm.

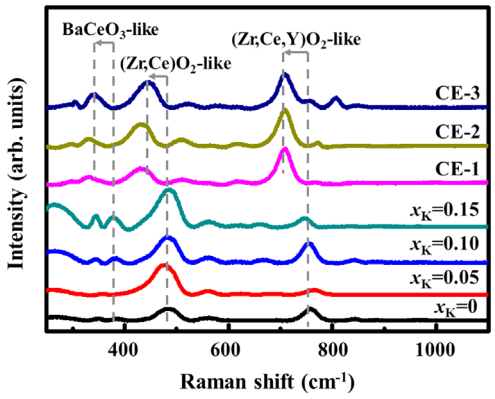

Fig. 6. Raman spectra of the sintered $Ba_{1-x}K_xCe_{0.6}Zr_{0.2}Y_{0.2}O_{3-\delta}$ oxides with different K doping contents prepared from conventional sol–gel or sol–gel combined with composition-exchange powders.

Raman spectroscopy can provide more useful information about the local configuration of chemical bonding in sintered $Ba_{1-x}K_xCe_{0.6}Zr_{0.2}Y_{0.2}O_{3-\delta}$ oxides. In our previous work, we reported that high phase homogeneity in $BaCe_{0.6}Zr_{0.2}Y_{0.2}O_{3-\delta}$ oxides can be achieved by adding an appropriate amount of Sr [32]. Fig. 6 shows the representative Raman spectra of all sintered pellets in this study. Several Raman-active modes, such as ZrO_2-like, CeO_2-like, and Y_2O_3-like phonon vibrations, have been reported in $BaCe_{1-x-y}Zr_xY_yO_{3-\delta}$ perovskites [33]. For the sintered pellets prepared from conventional sol–gel powders, the broad Raman peak around 485 cm^{-1} most likely corresponds to the $(Zr,Ce)O_2$-like vibration modes, since the major Raman peaks of CeO_2 and ZrO_2 powders locate at 461 and 474 cm^{-1}, respectively [34,35]. A broaden peak around 750 cm^{-1} associated with the $(Zr,Ce,Y)O_2$-like vibration mode is also observed [33]. We find that these phonon vibrations are shifted toward lower frequencies for the sintered pellets prepared from sol–gel combined with composition- exchange powders. This indicates that the composition-exchange process for calcined powders indeed influences the K doping behavior and configuration of chemical bonding in sintered $Ba_{1-x}K_xCe_{0.6}Zr_{0.2}Y_{0.2}O_{3-\delta}$ oxides. However, the exact mechanism needs to be further clarified. As shown in Fig. 7, Raman intensity of $(Zr,Ce)O_2$-like band is mapped over the 15%-K-doped sintered pellet pressed from conventional sol–gel powders and the CE-3 sample. It is evident that the 15%-K-doped sintered pellet reveals a non-uniform distribution of $(Zr,Ce)O_2$-like vibration intensity in the mapping region. On the contrary, for the CE-3 sample, the measured signal intensity is considerably uniform, showing high phase homogeneity in the sintered oxide. This result indicates that although the 15%-K-doped sintered pellet prepared from conventional sol–gel powders has higher ability to suppress the formation of CeO_2-like second phase as discussed in the XRD results, its spatial configuration of CeO_2-like chemical bonding is not homogenous, possibly due to non-uniform K loss from its highly porous structures. This useful information cannot be revealed in the above-discussed XRD results.

Electrolyte conduction directly affects the overall energy conversion performance of H^+-SOFCs. Here, the ionic conductivities of the sintered $Ba_{1-x}K_xCe_{0.6}Zr_{0.2}Y_{0.2}O_{3-\delta}$ pellets were evaluated as a function of temperatures in air atmosphere with 3% relative humidity. Fig. 8 summarizes the measurement data. The increase in conductivity with increasing temperature indicates that all sintered pellets exhibit ionic conduction. However, different K-doping dependences of conductivities are observed for the sintered pellets prepared by various methods. For the pellets from conventional sol–gel powders, the conductivity is increased to a maximal value by an addition of 5% K. It demonstrates that introducing highly basic alkaline cations into perovskite oxides indeed improve their conductivities. However, further increasing the K doping content more than 5% dramatically

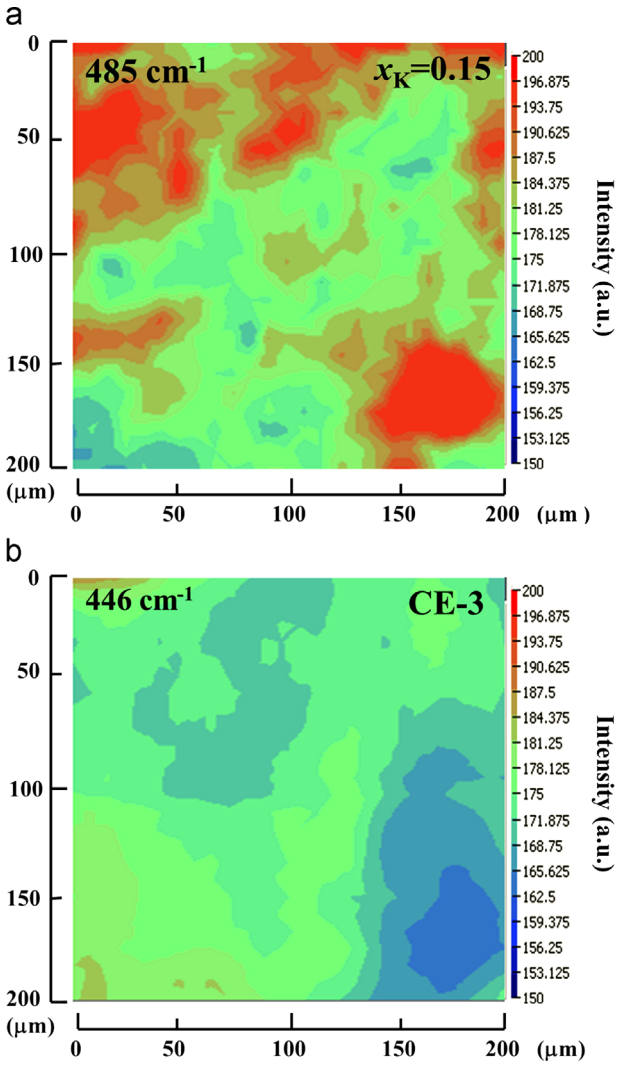

Fig. 7. Raman mapping of $(Zr,Ce)O_2$-like band on the (a) 15%-K-doped sintered $Ba_{1-x}K_xCe_{0.6}Zr_{0.2}Y_{0.2}O_{3-\delta}$ pellet and (b) CE-3 pellet.

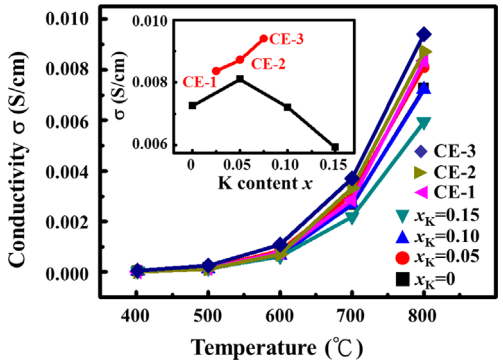

Fig. 8. Conductivities of the sintered $Ba_{1-x}K_xCe_{0.6}Zr_{0.2}Y_{0.2}O_{3-\delta}$ pellets prepared from conventional sol–gel or sol–gel combined with composition-exchange powders as a function of measuring temperatures.

decreases the oxide conductivity mainly due to high structural porosity. This trend is well consistent with SEM observations and measured relative densities. On the other hand, the conductivities of the sintered pellets prepared from sol–gel combined with composition-exchange powders show an increasing trend with the increasing K doping. Among all sintered pellets in this study, the $Ba_{0.925}K_{0.075}Ce_{0.6}Zr_{0.2}Y_{0.2}O_{3-\delta}$ pellet fabricated by this new method has the highest conductivity, 0.0094 S/cm at 800 °C, which is higher than those pressed from conventional sol–gel powders in the K doping range of 0–15%. This value is lower than that reported in $BaCe_{0.45}Zr_{0.45}Y_{0.1}O_{3-\delta}$ oxide (~0.0106 S/cm) [36], but is comparable to those of Sr-, In-, Gd-, Sm-, and Sc-doped $Ba(Ce,Zr)O_3$ electrolytes at the same temperature of 800 °C (Sr-doped: 0.009 S/cm, In-doped: 0.005 S/cm, Gd-doped: 0.0082 S/cm, Sm-doped: 0.0069 S/cm, and Sc-doped: 0.0027 S/cm) [32,36,37]. It is expected that this value can be further improved by tuning the experimental parameters. The related work is still in progress. Based on the above-discussed results, this enhanced conductivity in the pellets prepared from sol–gel combined with composition-exchange powders can be attributed to the denser microstructures and higher phase homogeneity in sintered oxides.

One major advantage of H^+-SOFCs over low-temperature polymer-electrolyte fuel cells (PEFCs) is the capable of using hydrocarbon fuels (instead of pure hydrogen). The hydrocarbon gas can be in-situ reformed into CO_2 and H_2 by the catalysts on the H^+-SOFC anodes. It is essential to ensure that the materials have thermodynamic or at least long-term kinetic stability in addition to good conductivity in the application environment for the electrolyte of H^+-SOFC. Therefore, the operational reliability of ceramic electrolytes in the CO_2- or H_2O-containing atmosphere is important. In order to verify the chemical stability, the CE-3 pellet was exposed to pure CO_2 in a tube furnace at 600 °C for long duration and the phase evolution was identified by XRD. It is found that the CE-3 pellet exhibits excellent chemical stability against CO_2 even after exposure to CO_2 for 16 h. As shown in Fig. 9, the XRD peaks from original perovskite phase remain almost unchanged and no decomposition of $Ba_{1-x}K_xCe_{0.6}Zr_{0.2}Y_{0.2}O_{3-\delta}$ into $BaCO_3$ or CeO_2 is detected. In recent stability work, the calcined $Ba(Ce_{0.8-x}Zr_x)Y_{0.2}O_{3-\delta}$ powders synthesized by sol–gel exhibit sufficient chemical stability for $x > 0.5$ when exposed to CO_2 atmosphere at 900 °C for 3 h [18]. Similarly, Guo et al. also studied the chemical stability of $BaZr_yCe_{0.8-y}Y_{0.2}O_{3-\delta}$, indicating that if $y < 0.4$, the perovskite structure is destroyed in CO_2 atmosphere at 650 °C for 2 h [16]. Moreover, a reliable and

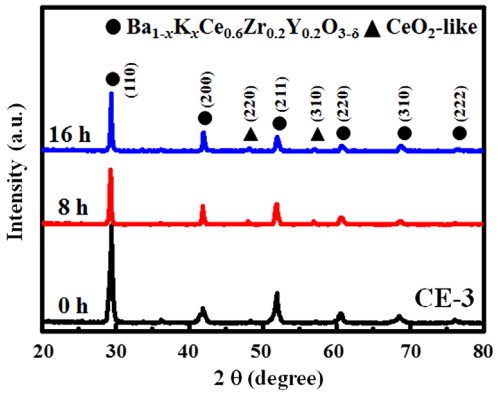

Fig. 9. XRD patterns of the CE-3 pellet after exposure to CO_2 atmosphere at 600 °C for 0 h, 8 h and 16 h.

favorable device performance has been demonstrated for the operation of single cells using these $Ba(Ce_{0.8-x}Zr_x)Y_{0.2}O_{3-\delta}$ oxides as electrolytes. Therefore, the sintered $Ba_{1-x}K_xCe_{0.6}Zr_{0.2}Y_{0.2}O_{3-\delta}$ oxides synthesized in the present study, which have shown excellent resistance to CO_2 for 16 h, are supposed to possess sufficient chemical stability and reliability in the H^+-SOFC operation environment. Tests of single cells using $Ba_{1-x}K_xCe_{0.6}Zr_{0.2}Y_{0.2}O_{3-\delta}$ as electrolyte are still ongoing and will be discussed elsewhere.

4. Conclusions

In conclusion, this study first investigates the synthesis of $Ba_{1-x}K_xCe_{0.6}Zr_{0.2}Y_{0.2}O_{3-\delta}$ oxides by sol–gel combined with the composition-exchange method. Compared to the sintered oxides prepared from conventional sol–gel powders, $Ba_{1-x}K_xCe_{0.6}Zr_{0.2}Y_{0.2}O_{3-\delta}$ oxides synthesized by sol–gel combined with the composition-exchange method exhibit improved sinterability, higher conductivity, more homogeneous phase, and excellent chemical stability against CO_2. Among all sintered oxides in this study, the $Ba_{0.925}K_{0.075}Ce_{0.6}Zr_{0.2}Y_{0.2}O_{3-\delta}$ pellet fabricated by this new method has the highest conductivity, 0.0094 S/cm at 800 °C, which is higher than those prepared from conventional sol–gel powders in the K doping range of 0–15%. Based on the experimental results, the mechanism for improvement in these properties is discussed in terms of calcined particle characteristics. This work shows that $Ba_{1-x}K_xCe_{0.6}Zr_{0.2}Y_{0.2}O_{3-\delta}$ oxides synthesized by sol–gel combined with the composition-exchange method would be a promising electrolyte for H^+-SOFC applications. More importantly, this new fabrication approach may be applied to other similar material systems, such as Sr- or Gd-doped $Ba(Ce,Zr)O_3$ perovskites.

Acknowledgments

The research is supported by National Nano-Device Laboratories and National Science Council of Taiwan under Contract nos. NSC 101-3113-P-008-006 and NSC 100-2221-E-008-016-MY3 respectively. The authors also thank National Nano-Device Laboratories and Center for Nano-Science and Technology at National Central University for the facility support.

References

[1] E.P. Murray, T. Tsai, S.A. Barnett, A direct-methane fuel cell with a ceria-based anode, Nature 400 (1999) 649–651.
[2] A. Arabacı, M.F. Öksüzömerb, Preparation and characterization of 10 mol% Gd doped CeO_2 (GDC) electrolyte for SOFC applications, Ceramics International 38 (2012) 6509–6515.
[3] Y.H. Zhang, X.Q. Huang, Z. Lu, Z.G. Liu, X.D. Ge, J.H. Xu, X.S. Xin, X.Q. Sha, W.H. Su, A study of the process parameters for yttria-stabilized zirconia electrolyte films prepared by screen-printing, Journal of Power Sources 160 (2006) 1065–1073.
[4] J.FW. Fergus, Electrolytes for solid oxide fuel cells, Journal of Power Sources 162 (2006) 30–40.
[5] I.M. Hung, H.W. Peng, S.L. Zheng, C.P. Lin, J.S. Wu, Phase stability and conductivity of $Ba_{1-y}Sr_yCe_{1-x}Y_xO_{3-\delta}$ solid oxide fuel cell electrolyte, Journal of Power Sources 193 (2009) 155–159.
[6] X.W. Chi, J.C. Zhang, M.F. Wu, Y. Liu, Z.Y. Wen, Study on stability and electrical performance of yttrium and bismuth co-doped $BaCeO_3$, Ceramics International 39 (2013) 4899–4906.
[7] L. Yang, C.D. Zuo, S.H. Wang, Z. Cheng, M. Liu, A novel composite cathode for low-temperature SOFCs based on oxide proton conductors, Advanced Materials 20 (2008) 3280–3283.
[8] A. Radojković, M. Žunić, S.M. Savić, G. Branković, Z. Branković, Chemical stability and electrical properties of Nb doped $BaCe_{0.9}Y_{0.1}O_{3-\delta}$ as a high temperature proton conducting electrolyte for IT-SOFC, Ceramics International 39 (2013) 307–313.
[9] M. Zhang, W.S. Yang, Direct ammonia solid oxide fuel cell based on thin proton-conducting electrolyte, Journal of Power Sources 179 (2008) 92–95.
[10] K.D. Kreuer, Solid State Ionics 97 (1997) 1–15.
[11] H. Iwahara, Technological challenges in the application of proton conducting ceramics, Solid State Ionics 77 (1995) 289–298.
[12] T. Shimada, C. Wen, N. Taniguchi, J. Otomo, H. Takahashi, The high temperature proton conductor $BaZr_{0.4}Ce_{0.4}I_{0.2}O_{3-\delta}$, Journal of Power Sources 131 (2004) 289–292.
[13] F. Zhao, F.L. Chen, Performance of solid oxide fuel cells based on proton-conducting $BaC_{e0.7}In_{0.3-x}Y_xO_{3-\delta}$, International Journal of Hydrogen Energy 35 (2010) 11194–11199.
[14] F. Zhao, Q. Liu, S.W. Wang, K. Brinkman, F.L. Chen, Synthesis and characterization of $BaIn_{0.3-x}Y_xCe_{0.7}O_{3-\delta}$ (x=0, 0.1, 0.2, 0.3) proton conductors, International Journal of Hydrogen Energy 35 (2010) 4258–4263.
[15] J.D. Lu, L. Wang, L.H. Fan, Y.H. Li, L. Dai, H.X. Guo, Chemical stability of doped $BaCeO_3$–$BaZrO_3$ solid solutions in different atmospheres, Journal of Rare Earths 26 (2008) 505–510.
[16] Y.M. Guo, Y. Lin, R. Ran, Z.P. Shao, Zirconium doping effect on the performance of proton-conducting $BaZr_yCe_{0.8-y}Y_{0.2}O_{3-\delta}$ ($0.0 \le y \le 0.8$) for fuel cell applications, Journal of Power Sources 193 (2009) 400–407.
[17] Z.T. Tao, Z.W. Zhu, H.Q. Wang, W. Liu, A stable $BaCeO_3$-based proton conductor for intermediate-temperature solid oxide fuel cells, Journal of Power Sources 195 (2010) 3481–3484.
[18] E. Fabbri, A. D′Epifanio, E.D. Bartolomeo, S. Licoccia, E. Traversa, Tailoring the chemical stability of $Ba(Ce_{0.8-x}Zr_x)Y_{0.2}O_{3-\delta}$ protonic conductors for intermediate temperature solid oxide fuel cells (IT-SOFCs), Solid State Ionics 179 (2008) 558–564.
[19] A. Magrasó, C. Frontera, A.E. Gunnæs, A. Tarancón, D. Marrero-López, T. Norby, R. Haugsrud, Structure, chemical stability and mixed proton–electron conductivity in $BaZr_{0.9-x}Pr_xGd_{0.1}O_{3-\delta}$, Journal of Power Sources 196 (2011) 9141–9417.
[20] X.L. Zhou, L.M. Liu, J.M. Zhen, S.C. Zhu, B.W. Li, K.N. Sun, P. Wang, Ionic conductivity, sintering and thermal expansion behaviors of mixed ion conductor $BaZr_{0.1}Ce_{0.7}Y_{0.1}Yb_{0.1}O_{3-\delta}$ prepared by ethylene diamine tetraacetic acid assisted glycine nitrate process, Journal of Power Sources 196 (2011) 5000–5006.
[21] K.H. Ryu, S.M. Haile, Chemical stability and proton conductivity of doped $BaCeO_3$–$BaZrO_3$ solid solutions, Solid State Ionics 125 (1999) 355–367.
[22] P. Babilo, T. Uda, S.M. Haile, Processing of yttrium-doped barium zirconate for high proton conductivity, Journal of Materials Research 22 (2007) 1322–1330.
[23] R.B. Cervera, Y. Oyama, S. Yamaguchi, Low temperature synthesis of nanocrystalline proton conducting $BaZr_{0.8}Y_{0.2}O_{3-\delta}$ by sol–gel method, Solid State Ionics 178 (2007) 569–574.
[24] H.G. Gu, R. Ran, W. Zhou, Z.P. Shao, Anode-supported ScSZ-electrolyte SOFC with whole cell materials from combined EDTA–citrate complexing synthesis process, Journal of Power Sources 172 (2007) 704–712.
[25] N.H. Perry, S. Kim, T.O. Mason, Local electrical and dielectric properties of nanocrystalline yttria-stabilized zirconia, Journal of Materials Science 43 (2008) 4684–4692.
[26] A.S. Patnaik, A.V. Virkar, Transport properties of potassium-doped $BaZrO_3$ in oxygen- and water-vapor-containing atmospheres, Journal of the Electrochemical Society 153 (2006) A1397–A1405.

[27] X.X. Xu, S.W. Tao, J.T.S. Irvine, Proton conductivity of potassium doped barium zirconates, Journal of Solid State Chemistry 181 (2008) 93–98.

[28] C.S. Tu, R.R. Chien, V.H. Schmidt, S.C. Lee, C.C. Huang, C.L. Tsai, Thermal stability of $Ba(Zr_{0.8-x}Ce_xY_{0.2})O_{2.9}$ ceramics in carbon dioxide, Journal of Applied Physics 105 (2009) 103504.

[29] Y. Zeng, P.L. Mao, S.P. Jiang, P. Wu, L. Zhang, P. Wu, Prediction of oxygen ion conduction from relative Coulomb electronic interactions in oxyapatites, Journal of Power Sources 196 (2011) 4524–4532.

[30] J.S. Park, J.K. Lee, K.S. Hong, The effect of alkali niobate addition on the phase stability and dielectric properties of $Pb(Zn_{1/3}Nb_{2/3})O_3$ based ceramic, Journal of Applied Physics 101 (2007) 114101–114107.

[31] X.C. Liu, R. Hong, C. Tian, Tolerance factor and the stability discussion of ABO_3-type ilmenite, Journal of Materials Science: Materials in Electronics 20 (2009) 323–327.

[32] K.R. Lee, C.J. Tseng, J.K. Chang, I.M. Hung, J.C. Lin, S.W. Lee, Strontium doping effect on phase homogeneity and conductivity of $Ba_{1-x}Sr_xCe_{0.6}Zr_{0.2}Y_{0.2}O_{3-\delta}$ proton-conducting oxides, International Journal of Hydrogen Energy 38 (2013) 11097–11103.

[33] R.R. Chien, C.S. Tu, V.H. Schmidt, S.C. Lee, C.C. Huang, Synthesis and characterization of proton-conducting $Ba(Zr_{0.8-x}Ce_xY_{0.2})O_{2.9}$ ceramics, Solid State Ionics 181 (2010) 1251–1267.

[34] R.Q. Long, Y.P. Huang, H.L. Wan, Surface oxygen species over cerium oxide and their reactivities with methane and ethane by means of in situ confocal microprobe Raman spectroscopy, Journal of Raman Spectroscopy 28 (1997) 29–32.

[35] B.K. Kim, H.O. Hamaguchi, Mode assignments of the Raman spectrum of monoclinic zirconia by isotopic exchange technique, Physica Status Solidi B 203 (1997) 557–563.

[36] J. Lv, L. Wang, L. Dai, H. Guo, R.V. Kumar, Sintering, chemical stability and electrical conductivity of the perovskite proton conductors $BaCe_{0.45}Zr_{0.45}M_{0.1}O_{3-\delta}$ (M=In, Y, Gd, Sm), Journal of Alloys and Compounds 467 (2009) 376–382.

[37] A.K. Azad, J.T.S. Irvine, Synthesis, chemical stability and proton conductivity of the perovksites $Ba(Ce,Zr)_{1-x}Sc_xO_{3-\delta}$, Solid State Ionics 178 (2007) 635–640.